Geol. Mag. **144** (*2*), *2007, pp. 271–287.* © *2007 Cambridge University Press*

doi:10.1017/S0016756806002998 First published online 4 January 2007 *Printed in the United Kingdom*

Microstructures in a banded iron formation (Gua mine, India)

MANISH A. MAMTANI*, A. MUKHERJI & A. K. CHAUDHURI

Department of Geology & Geophysics, Indian Institute of Technology, Kharagpur-721302, India

(*Received* 20 October 2005; *accepted* 10 May 2006)

Abstract – This paper provides a detailed documentation of microstructures developed in the banded iron formation (BIF) of Gua mine, located in the Bonai Synclinorium (eastern India), where the rocks have been subjected to three deformations (D_1 to D_3). Folded iron ores, quartz strain fringes around rigid core objects and folded iron ore layers, and refracted quartz veins are described from samples taken from D_2 folds in the banded iron formation. Orientations of microstructures are compared with mesoscopic structures to interpret the generations of ore minerals, planar structures and the time relationship between deformation and development of different microstructures. The mechanism of D_2 folding is worked out and its bearing on microstructure development is discussed. The D_2 folds are inferred to have developed by a combination of tangential longitudinal strain in the competent layer, flexural flow in the incompetent layers and flexural slip at the interface between layers of differing competence. Homogeneous flattening strain superposed the earlier strain, which led to modification of the folds in the competent layer from class 1B to 1C. This strain is quantified and is found to be higher in the limb than the hinge of a fold. Diffusive mass transfer by solution and bulging dynamic recrystallization in quartz are inferred as the dominant deformation processes during folding. Moreover, based on comparison with published deformation microstructure maps, the microstructures of the present study are estimated to have developed between 300 and 350 °C temperatures at a strain rate of 10^{-14}–10^{-12} s^{-1}, which are geologically realistic conditions for naturally deformed rocks.

Keywords: microstructure, banded iron formations, quartz, pressure solution, recrystallization, strain, folding.

1. Introduction

Banded iron formations (BIFs) are stratigraphically important rock types that occur in Precambrain terrains in different parts of the world, such as India, Australia and Brazil, among others. There have been many studies on BIFs with regard to understanding their genesis (e.g. Castro, 1994; Stolz, Lovely & Haggerty, 1990) and structural geology (e.g. Chauvet *et al.* 1994; Chemale, Rosière & Endo, 1994). In comparison to the field-based and chemical studies of BIFs, microstructural studies have been scarce. Development of textures and microstructures in hematite in BIFs has recently been investigated in detail using the neutron diffraction technique (e.g. Rosière *et al.* 2001; Siemes *et al.* 2003). Also, Hippertt, Lana & Takeshita (2001) discussed the deformation mechanisms that operated during folding of the Proterozoic BIF of the Quadrilátero Ferrífero granite–greenstone terrain (SE Brazil). However, other than the above, there has been very little study of microstructures in BIFs and it would not be wrong to state that (a) microstructures in BIFs are not well documented and (b) the time relationship between evolution of microstructures and mesoscopic structures is not widely investigated in BIFs. Further, there exists a volume of literature on processes involved in microstructure development (Passchier & Trouw, 1996 and references therein). Similarly, there are considerable studies on the mechanism of folding and phenomena such as cleavage refraction (Ramsay, 1962, 1967; Treagus, 1983; Ramsay & Huber, 1987). Microstructures and microstructural processes in folded rocks are expected to be intricately related to the mechanism of folding because the former must evolve progressively with folding. However, an integrated study of folds, mechanism of folding and microstructure development has rarely been attempted, especially on BIFs. The present paper focuses on this particular aspect. A detailed documentation of microstructures observed in the Archaean-age BIF of eastern India is provided and the deformation processes that resulted in their genesis are discussed. The classes of folds developed in layers of different competence that comprise the folded BIF samples are identified and the mechanism of folding is worked out. Orientations of the planar mesoscopic as well as microscopic structures in the BIF are discussed and the development of microstructures is inferred in light of the fold mechanism. Thus, the present paper is, to the best of the knowledge of the authors, one of the first attempts in a BIF that integrates microstructure development with the mechanism of folding.

*Author for correspondence: mamtani@gg.iitkgp.ernet.in

2. Geological setting and deformational history

The banded iron formation of eastern India occurs in the Singhbhum Orissa Iron Ore Craton, which extends over an area of around 40 000 km^2. It is bounded by the arcuate Singhbhum Shear Zone in the north and the Sukinda Thrust in the south (Saha, Ray & Sarkar, 1988). The Singhbhum Orissa Iron Ore Craton has a long Archaean history that has been discussed in detail by Saha (1994, p. 310), which is as follows. The oldest rocks are designated as the Older Metamorphic Group, which consists of medium-grade (amphibolite facies) pelitic schists, arenites, calc-schists, ortho- and para-amphibolites. Their deposition took place at 3.8 Ga. The Older Metamorphic Group rocks are intruded by biotite hornblende tonalite gneiss that is referred to as the Older Metamorphic Tonalite Gneiss. This intrusion along with folding of the Older Metamorphic Group rocks took place at *c.* 3.7–3.6 Ga, and subsequently between 3.5 and 3.4 Ga the Older Metamorphic Group as well as Older Metamorphic Tonalite Gneiss rocks were further deformed and folded. This was accompanied by thickening of the crust and led to partial melting and generation of Singhbhum Granite-A at 3.3 Ga. At 3.2 Ga, extension in the region led to the formation of elongated basins, in which eruption of huge volumes of acid to intermediate volcanics took place along with the deposition of BIF, that comprise the Iron Ore Group. Subsequently, at *c.* 3.1 Ga, the Iron Ore Group rocks were folded and slightly metamorphosed, and the basal parts of the sialic crust underwent partial melting to give rise to Singhbhum Granite-B.

The present study has been done on the BIF of the Bonai Synclinorium, which is one of the three elongated basins that was formed at around 3.2 Ga and is the type area of the folded Archaean Iron Ore Group. It comprises low-grade metasediments including phyllites, tuffaceous shales and banded hematite jaspers/banded hematite quartzites with iron ore. The thickness of the Iron Ore Group is around 350 m (Das *et al.* 1996). As stated above, the Iron Ore Group rocks are folded. However, they are only weakly metamorphosed, and according to Das *et al.* (1996), these BIFs were never subjected to temperatures above 200 °C. Structurally, the Bonai Synclinorium is horseshoe-shaped and on the map scale this shape is well defined by the BIF with several important open cast iron ore mines located at Gua, Bolani, Khandadhar, Sakradih, Patabeda, Khandbandh, Jururi, Joda and Noamundi (Fig. 1). Regionally, it is a gently NNE-plunging synclinorium that is overturned towards the east. The deformation history of the BIF of the Bonai Synclinorium has already been worked out in detail by Mukherji, Chaudhuri & Mamtani (2004) and therefore is only briefly summarized here.

A superposed fold history involving three phases of deformation, namely D_1, D_2 and D_3, has been worked

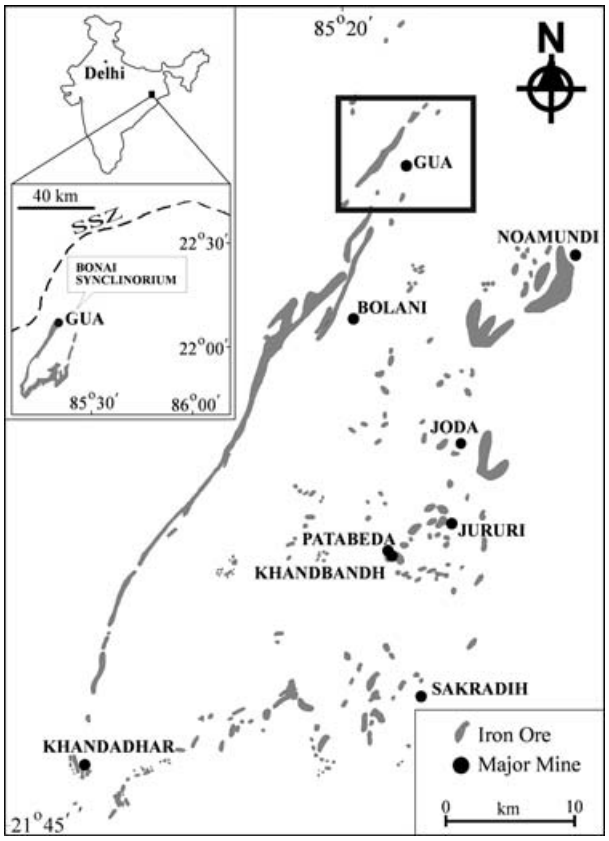

Figure 1. Location map of the study area in the Bonai Synclinorium (eastern India). The present microstructural investigation is concentrated on samples from the Gua mine, located on the western limb of the synclinorium (enclosed in the box). The inset map shows the regional location of the synclinorium. SSZ – Singhbhum Shear Zone. Map after Jones (1934).

out. D_1 deformation resulted in the development of folds that have a reclined to inclined geometry with fold axis lineations (L_1) trending in a NW–SE to N–S direction. The axial plane of D_1 folds, AP_1, varies in strike from NW–SE to NE–SW. D_2 deformation led to the development of open to tight D_2 folds with a fold axis trend varying between N–S and NNE–SSW. This near coaxial superposition of D_2 folds on D_1 resulted in the development of hook-shaped geometry or Type 3 interference patterns (Ramsay, 1967). The axial plane of D_2 folds, AP_2, is relatively straight and generally strikes in a N–S to NE–SW direction with steep dips. AP_1 is curved due to coaxial refolding by D_2. The fold axis lineations related to D_2 folds, L_2, are parallel to L_1. D_3 deformation that followed D_2 resulted in a cross-folding with the D_3 fold axis trending E–W to WNW–ESE. The D_3 folds are very broad, open and generally have an upright attitude with the axial plane (AP_3) striking E–W to WNW–ESE. At a few places, culminations and depressions of dome-basin Type 1 interference (Ramsay, 1967) are noted on the mesoscopic scale due to superposition of D_3 on D_1/D_2 folds. However, there are few mesoscopic structures related to D_3 and its effect is largely expressed by

https://doi.org/10.1017/S0016756806002998 Published online by Cambridge University Press

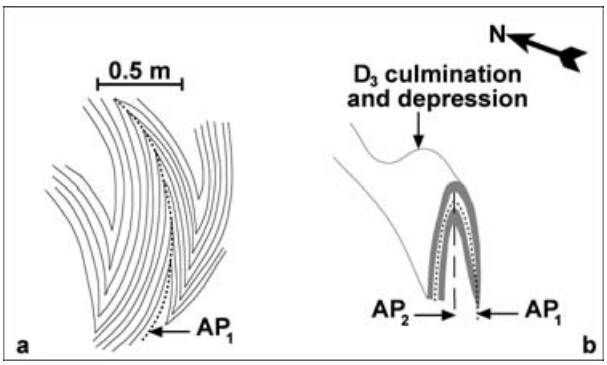

Figure 2. Sketches highlighting the style of folding of BIFs in the study area. (a) Coaxially refolded D_1 fold with curved axial trace (AP_1). (b) Three-dimensional schematic diagram documenting the coaxial geometry of D_1 and D_2 folds. Axial trace of D_1 (AP_1) is curved while axial trace of D_2 (AP_2) is straight. D_3 deformation followed D_2 and its superposition resulted in development of culminations and depressions, which resulted in variation in L_2 fold axis lineation.

variations in attitude of planar and linear elements of earlier generation structures. The above deformation history has been worked out on the basis of analyses of a large number of field planar and linear element data collected from the different mines located in the Bonai Synclinorium.

The microstructures described in the present paper are from the BIF samples of the Gua mine that is located on the western limb of the Bonai Synclinorium (box in Fig. 1). The fold history described above is supported by the structural observations from the Gua mine. Figure 2 shows sketches highlighting the style of folding, and Figure 3 shows the lower hemisphere equal area projections of structural elements recorded in this mine. The reader is referred to Mukherji, Chaudhuri & Mamtani (2004) for further details about structural analyses from the different mines of the Bonai Synclinorium.

3. Microstructures

Interesting microstructures such as folded ore minerals (e.g. hematite), refracted quartz veins, bedding-parallel quartz-shape fabric and quartz fringes are noted in the BIF (banded hematite jasper and banded hematite quartzite) of Gua mine. In this section a detailed documentation of the microstructures observed in the rocks is provided. Thin-sections of small-scale D_2 folds were also studied to compare the microstructures and orientations of fabric elements in the hinge and limb of folds and all the details are documented below.

3.a. Folded iron ore minerals

It is known from previous studies related to ore genesis (Majumdar & Chakraborty, 1979), rock magnetism (Das *et al.* 1996) and anisotropy of magnetic susceptibility (AMS) (Mukherji, Chaudhuri & Mamtani, 2004) of the BIF of the study area that hematite and magnetite are the dominant ore minerals in the rocks. However, an interesting observation is the presence of folded ore minerals around small-scale folds. Figure 4a shows a microfold from a banded hematite quartzite sample. It is found that the ore minerals occurring in the hinges of the folds are folded (Fig. 4a, b). In some samples, the ore minerals at the hinge have been reoriented and recrystallized into the axial planar direction of the folds (Fig. 4b, c). In contrast, ore minerals occurring on the limbs of small-scale folds are straight.

3.b. Refracted quartz veins

Refraction refers to the change in angle commonly observed in cleavage planes across lithological contacts, which is explained by changes in orientation of the XY plane in layers of different competencies (Ramsay, 1967, p. 404; Treagus, 1983). This causes, for example, a fanning of the cleavage around folds. In an antiformal structure, cleavage converges downwards in the competent layers and diverges downwards in incompetent layers (Ramsay, 1967, p. 405; Twiss & Moores, 1992, p. 246). Figure 5a shows a similar fanning and refraction of fractures filled with quartz, thus forming refracted quartz veins in a banded hematite jasper sample from Gua mine. Jaspery quartz (hardness on Moh's scale, H = 7) forms the more competent units while the iron ore layer that

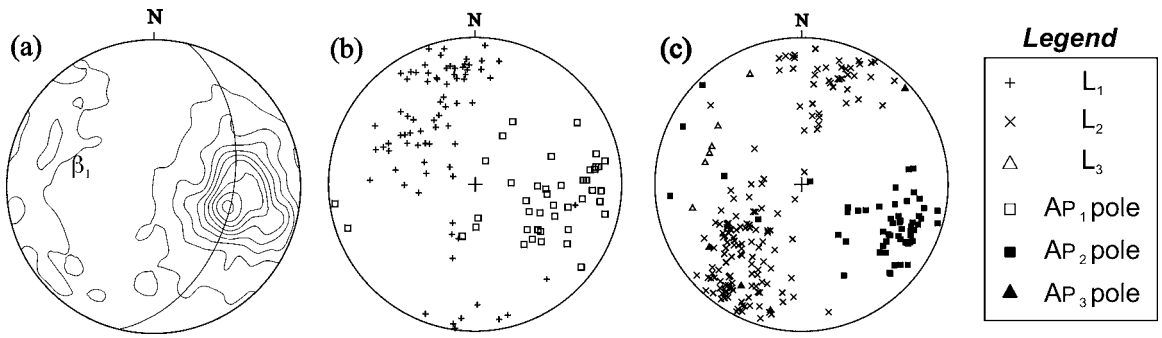

Figure 3. Lower hemisphere equal area projections of planar and linear field data recorded in the Gua mine. (a) Contoured π-diagram of bedding plane data (n = 986 S_0). Fold axis β_1 is at 45°/N285°. (b) D_1 structural elements: L_1 (n = 86) and AP_1 (n = 46 poles) data from Gua. (c) D_2 and D_3 structural elements: L_2 (n = 157), AP_2 (n = 58), L_3 (n = 6) and AP_3 (n = 4) data from Gua.

https://doi.org/10.1017/S0016756806002998 Published online by Cambridge University Press

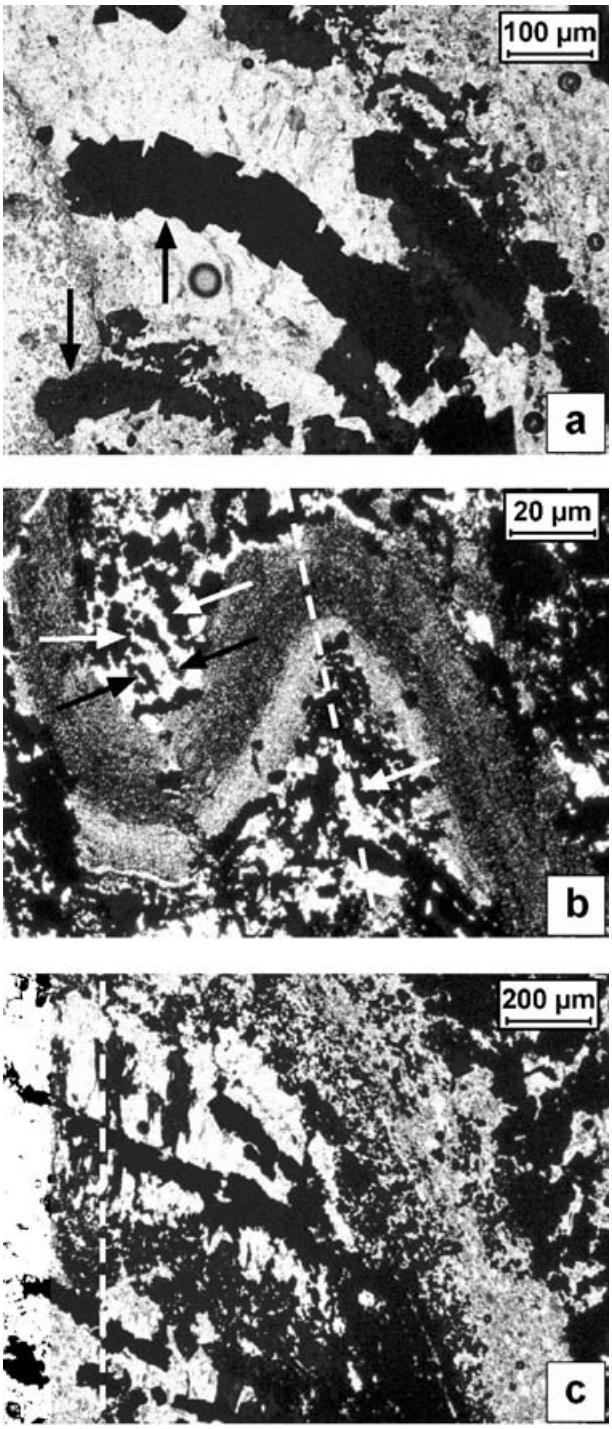

Figure 4. (a) Photomicrograph showing folded iron ores (arrows) in BIF from Gua mine (PPL). (b, c) Photomicrographs in PPL showing presence of reoriented and recrystallized iron ores (shown by arrows in b) in axial planar direction (dashed line).

dominantly consists of hematite (H = 5–6) comprises the incompetent unit. The sample is from a hinge of a D_2 fold. It may be noted that the refracted veins are restricted to a part that is proximal to the outer arc of the mesoscopic fold and are absent close to the inner arc. Figure 5b shows the quartz-filled fanning fractures at the microscopic scale. A drag effect (shown by arrows in Fig. 5b) is observed in quartz crystals at a few places, especially where the vein cuts through the incompetent layer (arrows in Fig. 5b); the fan is also noted to be divergent downwards at these localities. However, a similar drag effect is absent in the convergent part of the fan, where the quartz vein cuts through the competent layer.

This sample also has a quartz layer that lies between iron ore-rich layers. The quartz crystals in the quartz layer have a strong shape fabric that is parallel to the bedding plane (S_0 surface), which is the contact between the two different lithologies (Fig. 6a–c). It is to be noted that the quartz layer having a bedding-parallel fabric is folded, and this implies that the shape fabric is related to an earlier deformation event, the details of which are discussed in Section 4.b. The quartz crystals with the shape fabric are devoid of irregular grain boundaries and undulatory extinction, but are dominantly dentate (shown by white arrow in Fig. 6c). The quartz crystals that comprise the veins filling up the fanning fractures are coarser and have a weak to no shape-preferred orientation. The grain boundaries are dentate in many parts of the veins (shown by black arrow in Fig. 6c). However, at a few places, undulatory extinction and irregular bulging grain boundaries are also noted (Fig. 6d).

3.c. Strain fringes

Strain fringes are known to develop alongside rigid objects like ore minerals such as pyrite and magnetite crystals (Durney & Ramsay, 1973; Ramsay & Huber, 1983, p. 265; Etchecopar & Malavielle, 1987; Passchier & Trouw, 1996, p. 141; Ramsay & Lisle, 2000, p. 737). An object in a deforming matrix causes perturbations in the flow pattern and this may result in the growth of crystalline aggregates (fringes) close to the object in the direction of the extensional instantaneous stretching axes of flow. The central object between two strain fringes is termed a 'core object' and the whole structure (core object and fringes) is known as a 'fringe structure' (Koehn *et al.* 2000, 2001; Koehn, Bons & Passchier, 2003). Fringes can be 'syntaxial' (growth surface at matrix–fringe interface; core object and fringe are mineralogically similar), 'antitaxial' (growth surface at core object/fringe interface; core object is mineralogically different from the fringe) or 'composite' (combination of the first two). In the BIF of the present study area, anitaxial quartz strain fringes are prominently developed around rigid iron oxide core objects and interestingly also around folded iron ore layers. In the present section details of these fringes are documented.

3.c.1. Strain fringes around rigid core objects

Figures 7 and 8 highlight some of the interesting fringe structures noted in the rocks presently under

https://doi.org/10.1017/S0016756806002998 Published online by Cambridge University Press

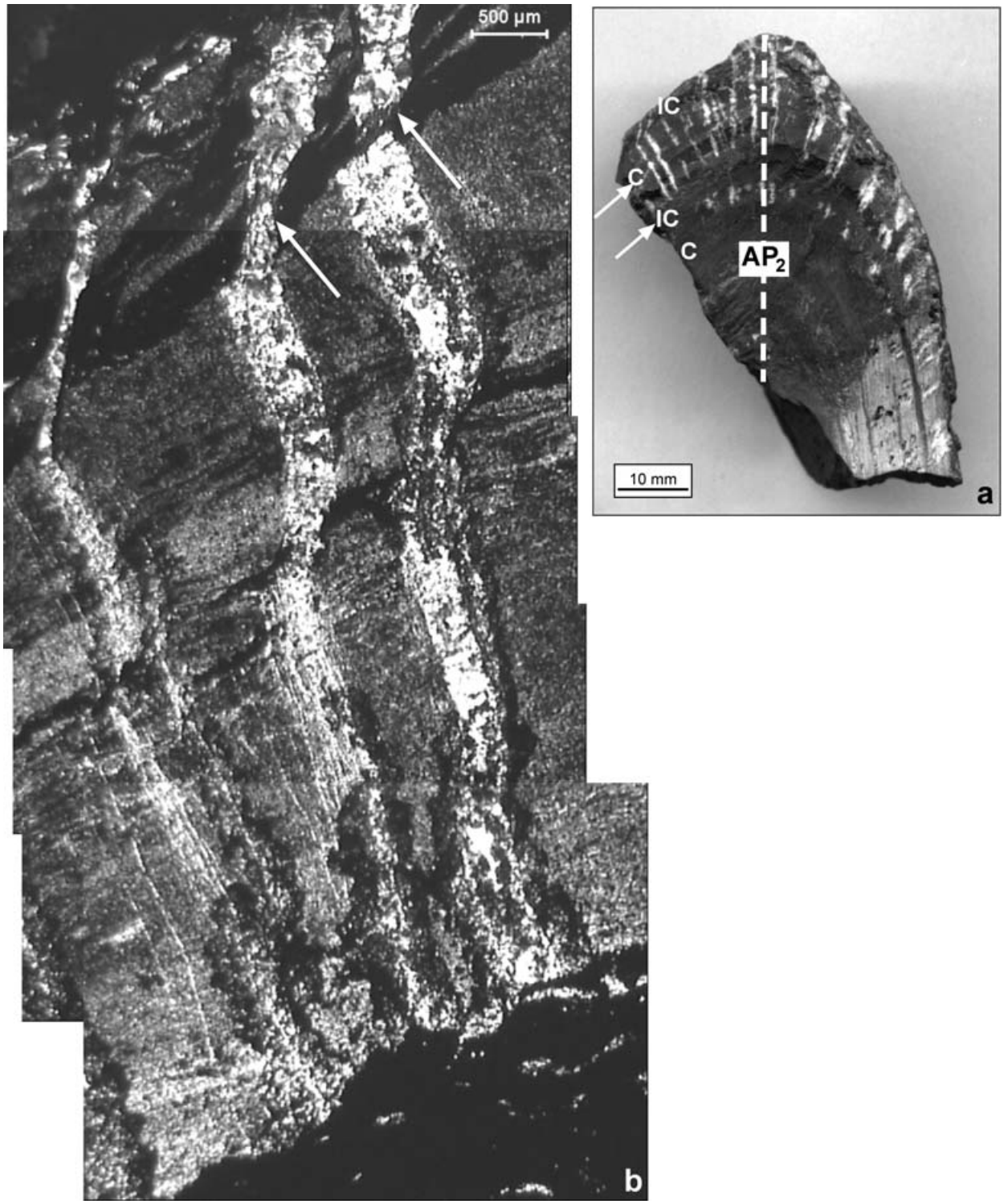

Figure 5. (a) Hand specimen of a folded banded hematite jasper sample from Gua mine showing refracted quartz veins. The sample is of a D_2 fold; IC and C indicate incompetent and competent layers respectively. The arrows point to the competent and incompetent layers that were used to determine the class of folds in Figure 11a–d. (b) Photomicrograph (mosaic) documenting refracted quartz veins. Arrows point to parts of the veins that show drag effect.

investigation. In some fringes the quartz fibres in contact with the core object are perpendicular to the core object (Fig. 7a). Such orientation is an indication of face-controlled growth (Ramsay & Huber, 1983; Passchier & Trouw, 1996). Most of the fringes, however, imply a displacement-controlled growth because fringes are oriented oblique to the core object (Figs 7b, 8a, b). Undulatory extinction as well as irregular

https://doi.org/10.1017/S0016756806002998 Published online by Cambridge University Press

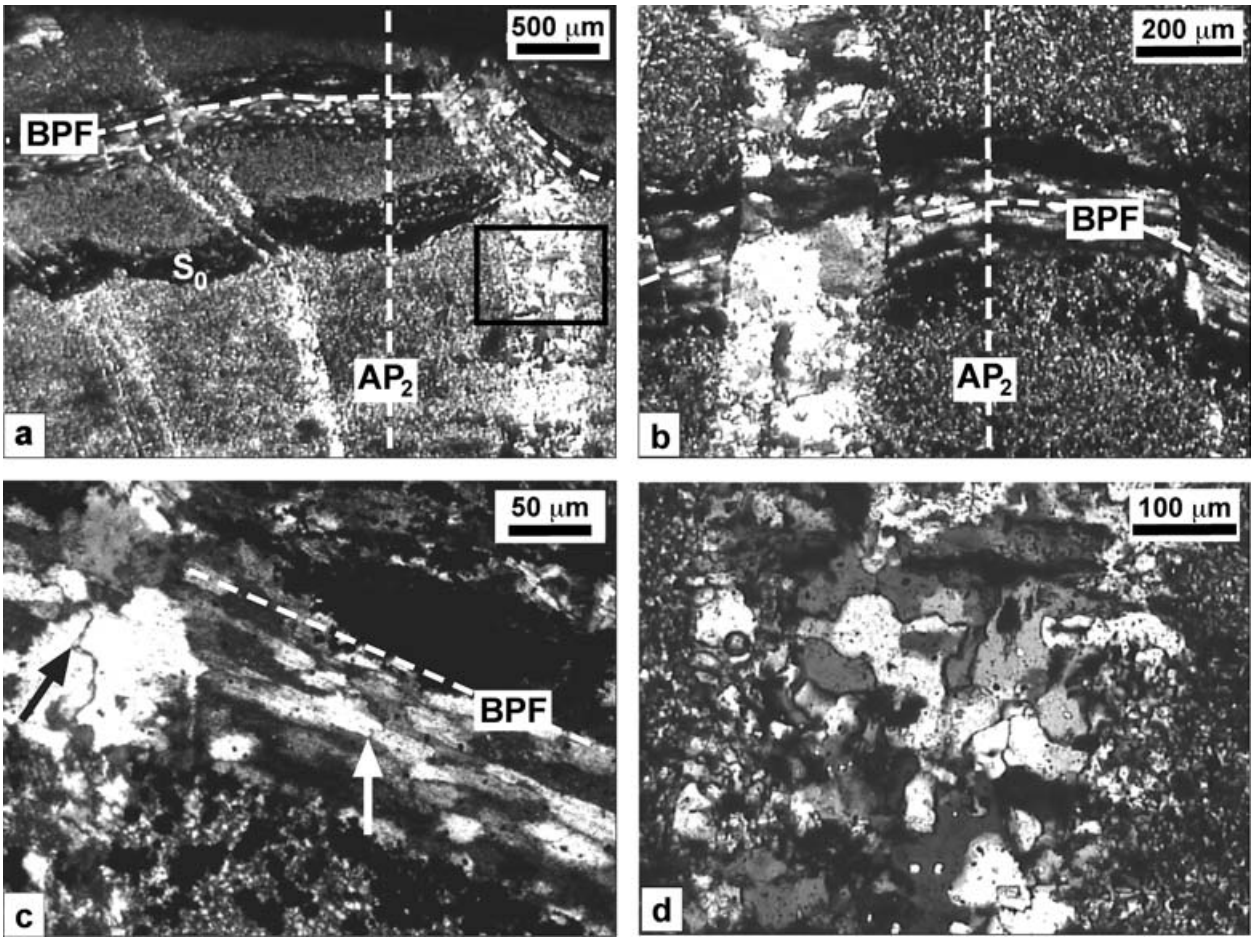

Figure 6. (a) Photomicrograph showing presence of a bedding-parallel fabric (BPF) defined by shape-preferred orientation of quartz crystals parallel to the layering (S_0) in a quartz layer within a banded hematite jasper from Gua mine. The bedding-parallel fabric is folded and its axial plane is AP_2. (b) Photomicrograph showing presence of interpenetrating grain boundaries between quartz crystals that comprise quartz veins. (c) Photomicrograph highlighting the absence of shape-preferred orientation in quartz veins that cut through the bedding-parallel fabric. Presence of dentate grain boundaries is noted along these veins (black arrow) as well as along quartz crystals that define the bedding-parallel fabric (white arrow). (d) Photomicrograph documenting presence of undulose extinction and irregular bulging grain boundaries within a part of quartz veins. This photomicrograph is an enlargement of the portion that is enclosed within the box in (a).

bulging grain boundaries are observed in the fringe quartz fibres. These are well documented in Figure 7c and also in the quartz fringes occupying the top left corner in Figure 7b. Moreover, there are some quartz crystals in this same sample that also show subgrains (Fig. 7d). Parts a and b of Figure 8 highlight quartz strain fringes observed in thin-sections of samples taken respectively from the hinge and limb of a hand-specimen scale D_2 fold (Fig. 8c). It is observed that the fibres in these samples are either straight or curved, with an average orientation parallel to the axial plane of the D_2 fold (AP_2). That the quartz strain fringes grow parallel to AP_2 in these BIFs is also well documented in Figure 8d and e; both these are from the hinge part of different samples from Gua mine. Figure 8f documents fringe structures noted away from the hinge in the same thin-section that contains the fringe structures in Figure 8e. It maybe noted that in Figure 8f all the strain fringes have grown parallel to the AP_2.

3.c.2. Strain fringes around folded iron ore layers

Similar to the fibres developed around core objects described above, strain fringes of quartz are also noted around folded iron ore layers and show variation in geometry and orientation around the fold (Figs 9, 10). Figure 9a is a mosaic of photomicrographs that clearly shows the above-mentioned variations around the folded layer. Orientations of fringes in different parts from the limb to the hinge of the fold are highlighted in Figure 9b–e, and Figure 10 is an explanatory sketch of the strain fringe geometry observed in Figure 9. It is observed that the strain fringes are straight in the limb of the fold and are oriented oblique to the iron ore layer, implying a displacement-controlled growth (Fig. 9b). The fringes are increasingly curved towards the hinge of the fold (Fig. 9c–e). Also, the thickness of the strain fringe zone (marked in Fig. 10) increases from the limb towards the hinge of the fold.

https://doi.org/10.1017/S0016756806002998 Published online by Cambridge University Press

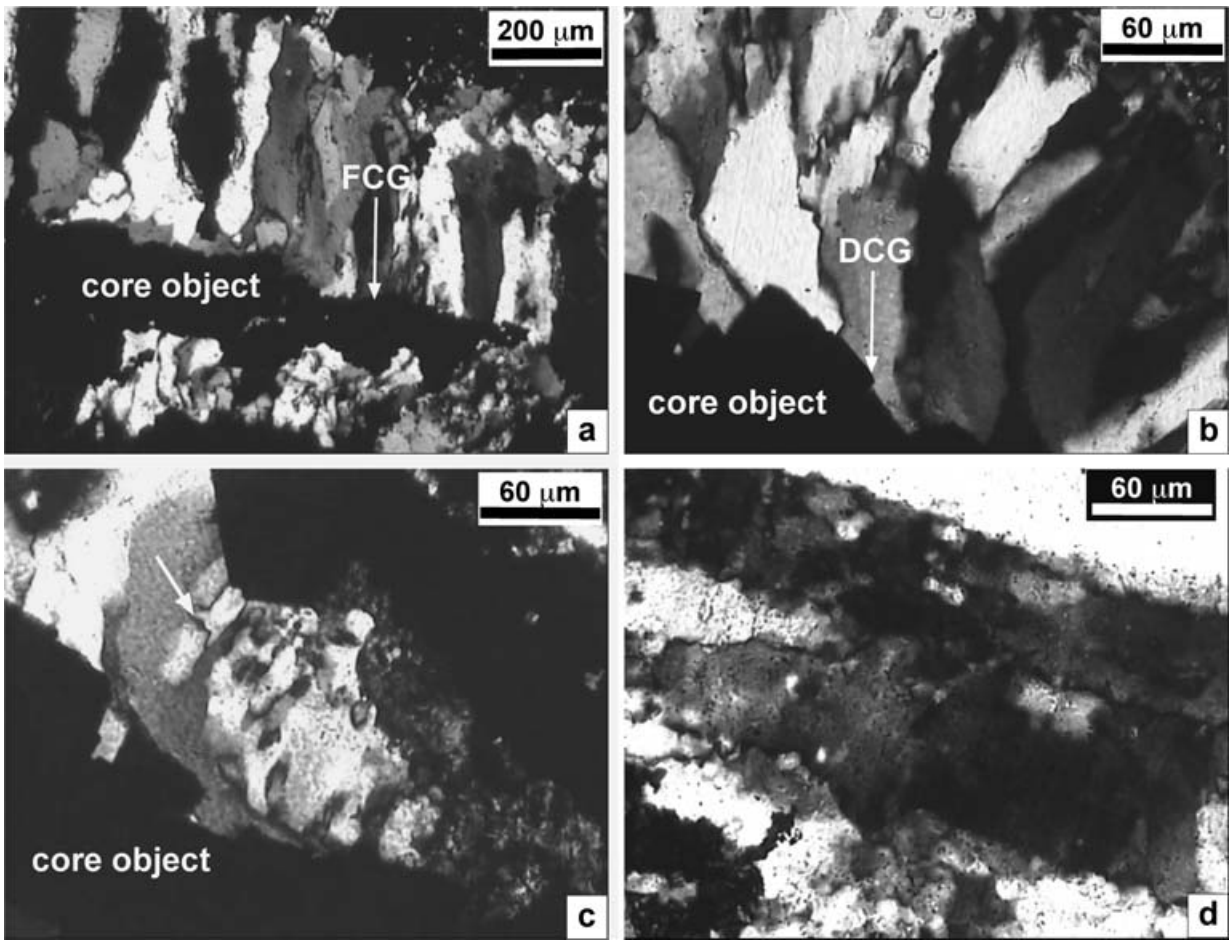

Figure 7. Photomicrographs of antitaxial quartz strain fringes around core object (iron oxide) in banded hematite quartzite from Gua mine. (a) and (b) respectively show face-controlled growth (FCG) and displacement-controlled growth (DCG) of quartz fringes around the core object. The presence of irregular grain boundaries and undulose extinction in quartz fringes is distinct in (b). Note that the surface of the core objects is irregular and consists of asperities. (c) Irregular bulging grain boundaries in quartz fringes implying bulging dynamic recrystallization. (d) Photomicrograph showing development of subgrains in quartz in the banded hematite quartzite sample.

4. Discussion

The above microstructures recorded in the BIF (banded hematite jasper and banded hematite quartzite) samples of the study area help in deciphering the time relationship between growth/recrystallization of minerals and deformation, dominant microscale deformation processes, and mechanism of folding, as well as estimation of temperature and strain rates; these are discussed below.

4.a. Generations of ore minerals

Microstructural studies have helped decipher the number of generations of iron ore minerals in the BIF samples. Since some iron ore minerals in the rocks are folded (Fig. 4a, b), it is concluded that the ore minerals formed prior to D_2 folding. However, Figure 4b–c also shows iron ore minerals in the hinge region of the fold that have grown in the axial planar direction. This indicates that although the ore minerals were present when the deformation/folding of the rocks began, they were subjected to some synkinematic recrystallization and reorientation, especially in the hinge parts of folds. This supplements the inference made from AMS studies by Mukherji, Chaudhuri & Mamtani (2004) that the BIF of the Bonai Synclinorium developed some tectonic fabric.

4.b. Generations of planar structures

BIFs (banded hematite jasper and banded hematite quartzite) are lithologies that do not easily develop a foliation. Therefore, axial plane foliation has not developed and is not recognizable in the field. The S-surface recorded in the field is the bedding plane (S_0). As stated earlier, wherever exposed, D_1 folds have a reclined geometry. Since D_2 was coaxial with D_1, this superimposition led to folding of axial surface of D_1 folds, refolding of S_0 and development of axial plane (AP_2). However, in several localities only the D_2 folds are preserved, and refolded D_1 folds are not well exposed. Therefore, deciphering the time relationship

https://doi.org/10.1017/S0016756806002998 Published online by Cambridge University Press

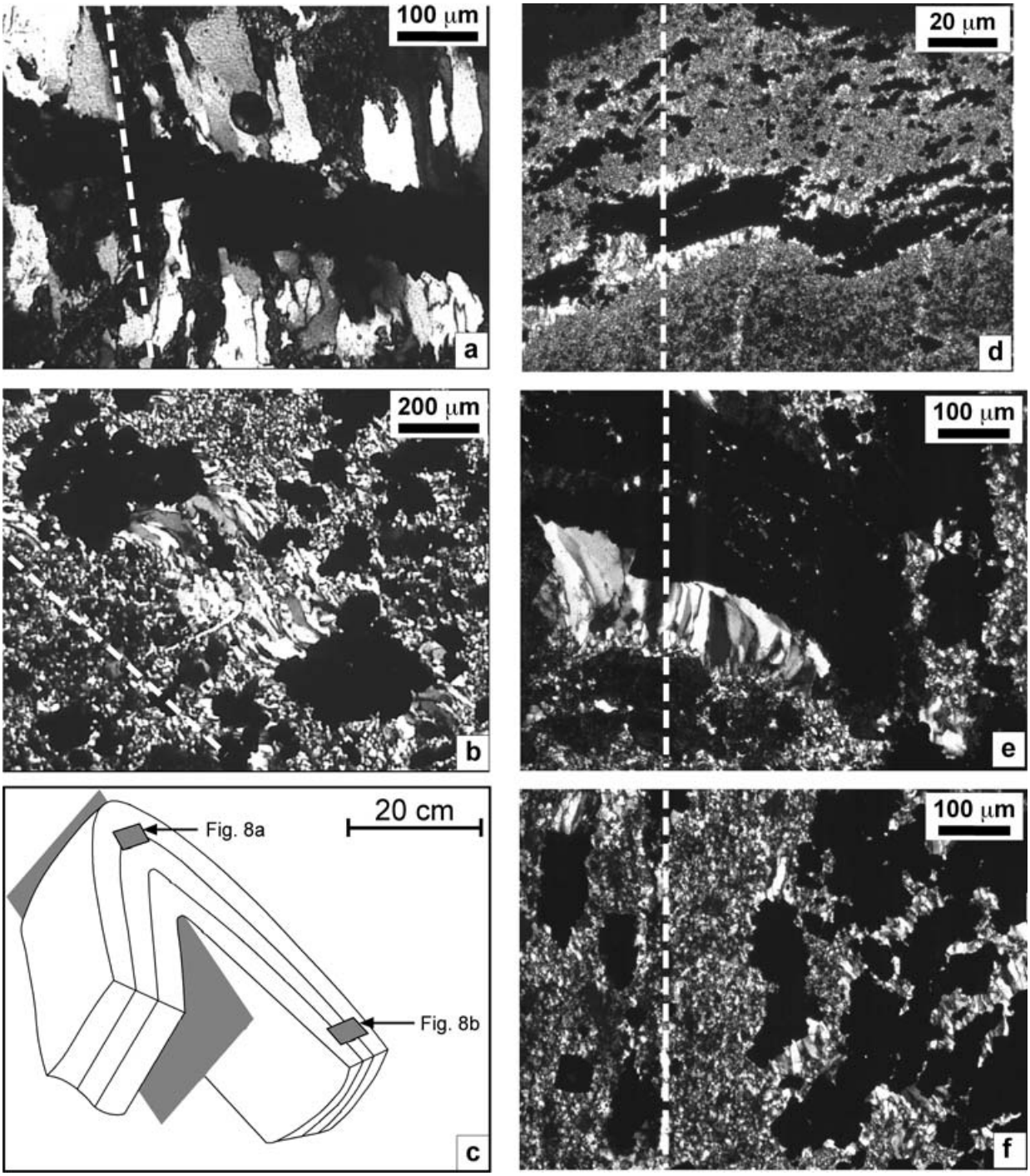

Figure 8. Photomicrographs of antitaxial quartz strain fringes around core objects (iron oxide) in various banded hematite quartzite samples from Gua mine. (a) is from the hinge while (b) is from the limb of a D_2 fold that is sketched in (c). Note the parallelism between orientation of the quartz fibres of the strain fringes and the axial plane direction, AP_2 (shown by dashed line). (d–f) are photomicrographs that document growth of quartz strain fringes parallel to AP_2 (dashed line) in other BIF samples from the study area. (e, f) are respectively from the hinge and limb of a single thin-section.

between deformation and fabric development in BIFs is often a challenge. Microstructural studies provide some evidence that helps in this regard. It is shown in Figure 6 that a bedding-parallel fabric defined by flattened quartz crystals has developed in the rocks and this is also folded. It has been suggested in an earlier study that extension veins close to the outer arc of a fold have radial geometry, while veins in the inner fold arc may form parallel to layer surfaces (Ramsay & Huber, 1987, p. 459). However, the bedding-parallel fabric documented in Figure 6 cannot be interpreted in accordance with the above because it is observed to have been cut by refracted fractures filled with quartz. This implies that the

https://doi.org/10.1017/S0016756806002998 Published online by Cambridge University Press

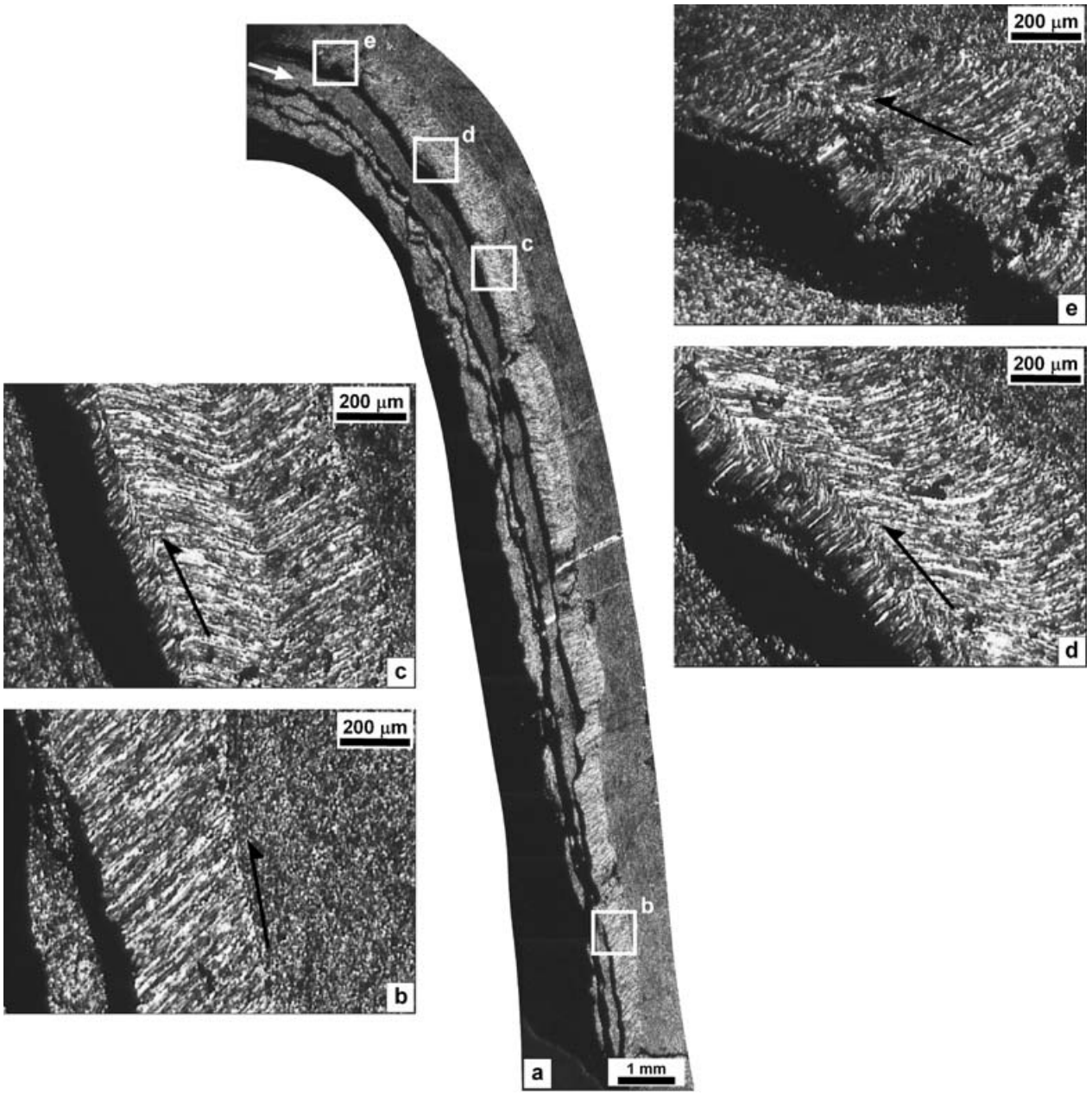

Figure 9. (a) Photomicrograph (mosaic) of a folded banded hematite jasper sample showing antitaxial quartz fringes around a folded iron ore layer. (b–e) Enlargements of areas that are enclosed within respectively marked boxes around the fold in (a). Arrow in the top left corner of (a) points to the competent layer that was used in Figure 11e, f to determine the fold class. Arrows in (b–e) point to the inferred movement direction from quartz fringe geometry in different parts of the fold. The thickness as well as curvature of the quartz fringes is greater in the hinge than the limb.

bedding-parallel fabric defined by the flattened quartz crystals developed prior to the development of the D_2 mesoscopic fold shown in Figure 5a. Therefore, it is inferred that the bedding-parallel fabric is a pre-D_2 fabric. However, in the absence of a properly exposed hinge of D_1 fold, the time relationship between deformation and development of the bedding-parallel fabric cannot be more accurately determined. There are two possibilities: (a) the bedding-parallel fabric may have developed prior to D_1 folding exclusively because of load or (b) it is syn-D_1 and the flattened quartz crystals may be considered to define a shape fabric that is equivalent to a S_1 fabric that was folded during D_2. If (a) were correct, then the bedding-parallel fabric would be designated as equivalent to S_0 and thus it would be concluded that Figure 6a–c highlights a S_0–AP_2 relationship from the hinge part of a D_2 fold. Moreover, under this condition the bedding-parallel fabric would have also been refolded by D_2 and the hinge of D_1 fold is the best place to observe this. Unfortunately, the latter is not well exposed. On the other hand if (b) (above) were valid, then the bedding-parallel fabric would be a tectonic fabric that may be designated as S_1 that is syn-D_1 in origin and was folded during D_2. In

https://doi.org/10.1017/S0016756806002998 Published online by Cambridge University Press

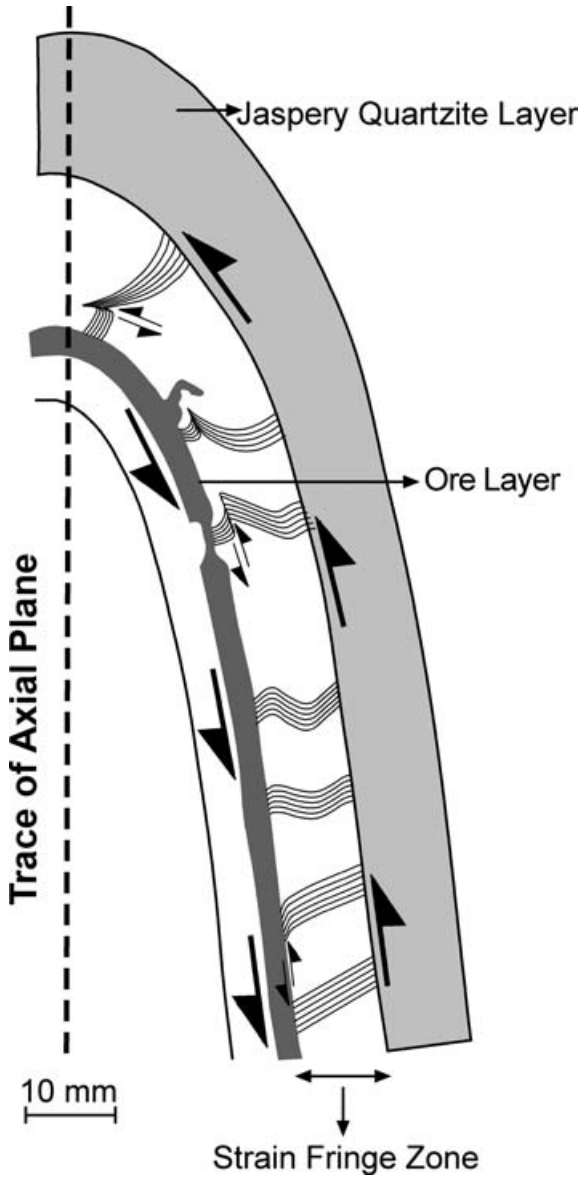

Figure 10. Sketch of thin-section of banded hematite jasper sample in Figure 9a. The arrows indicate the sense of shear in different parts of the fold inferred from the fringe geometry. The variation in the geometry of fringes around the folded iron ore layer is inferred to be related to the mechanism of folding, which is explained in Section 4.c.

this case, therefore, Figure 6a–c would be interpreted to highlight a S_1–AP_2 relationship. In either case, the bedding-parallel fabric is pre-D_2 in origin.

Since the above-described pre-D_2 structure (bedding-parallel fabric) is cut by fanned axial planar fractures, these must have developed later. From field studies, the fold is known to be D_2 and thus, the development of convergent and divergent fans observed in the competent and incompetent layers, respectively, are inferred to be synchronous with D_2 deformation. However, as stated in Section 3.b, these fanned fractures, wherever present, are restricted to a portion that forms the outer arc of mesoscopic folds and are filled with quartz, thus forming refracted quartz veins. This is inferred to be related to the mechanism of folding, the details of which are discussed in Section 4.c.

4.c. Mechanism of folding

The structures noted in the BIF samples have implications for inferring the mechanism of folding. It is known that when buckling of a layer takes place by tangential longitudinal strain, the distribution of strain within the layer is such that the outer arc undergoes extension and can develop extension fractures that may also be filled with fibres of quartz or calcite, while the inner arc undergoes compression and may develop minor crinkles; both these regions are separated by a neutral surface, which is a surface of no strain (Ramsay & Huber, 1987, p. 458). As shown in Figure 5a, the refracted quartz veins in the BIF presently under investigation are restricted to the outer arc of mesoscopic folds and are absent in the inner arc. This implies that buckling by tangential longitudinal strain must have been an important fold mechanism. However, multilayered rocks that buckle by this fold mechanism must develop class 1B folds in the competent units due to tangential longitudinal strain, while flexural flow in the incompetent layer results in class 3 folds (Ramsay, 1967; Twiss & Moores, 1992; Ghosh, 1993).

The authors have prepared t' ($=t_\alpha/t_0$) v. α and T' ($=T_\alpha/T_0$) v. α plots for some of the layers of the folds documented in Figures 5a and 9a (Fig. 11). Here α is the angle between the tangent to the folded surface at any point and the line normal to the axial surface trace, T is the axial trace thickness and t is the orthogonal thickness (Ramsay, 1967). The plots for the competent layer (Fig. 11a, b, e, f) reveal that the folds belong to class 1C. The plots for the incompetent layer (Fig. 11c, d) indicate that the folds in them are class 3. While it is expected that incompetent layers must have a class 3 geometry, the competent layers should ideally develop class 1B folds. This indicates that there must have been a superposition of some other type of strain during the later stages of folding that modified the folds during progressive deformation. Ramsay (1962, 1967) referred to such folds as 'flattened parallel folds' and demonstrated that superposition of homogeneous flattening over a class 1B fold modifies it to class 1C. A similar superposition over a class 3 fold leaves it within class 3 but with a tendency to approach class 2 fold geometry. This is quite clear in Figure 11c for the incompetent layer, where the curve deviates only slightly from the line at $T' = 1.0$ that demarcates class 2 folds. Thus it is inferred that in the BIF of the study area, tangential longitudinal strain was superposed by homogeneous flattening. Moreover, as shown by Ramsay (1962, 1967), the t' v. α and T' v. α plots can also be used to quantify the amount of homogeneous flattening

https://doi.org/10.1017/S0016756806002998 Published online by Cambridge University Press

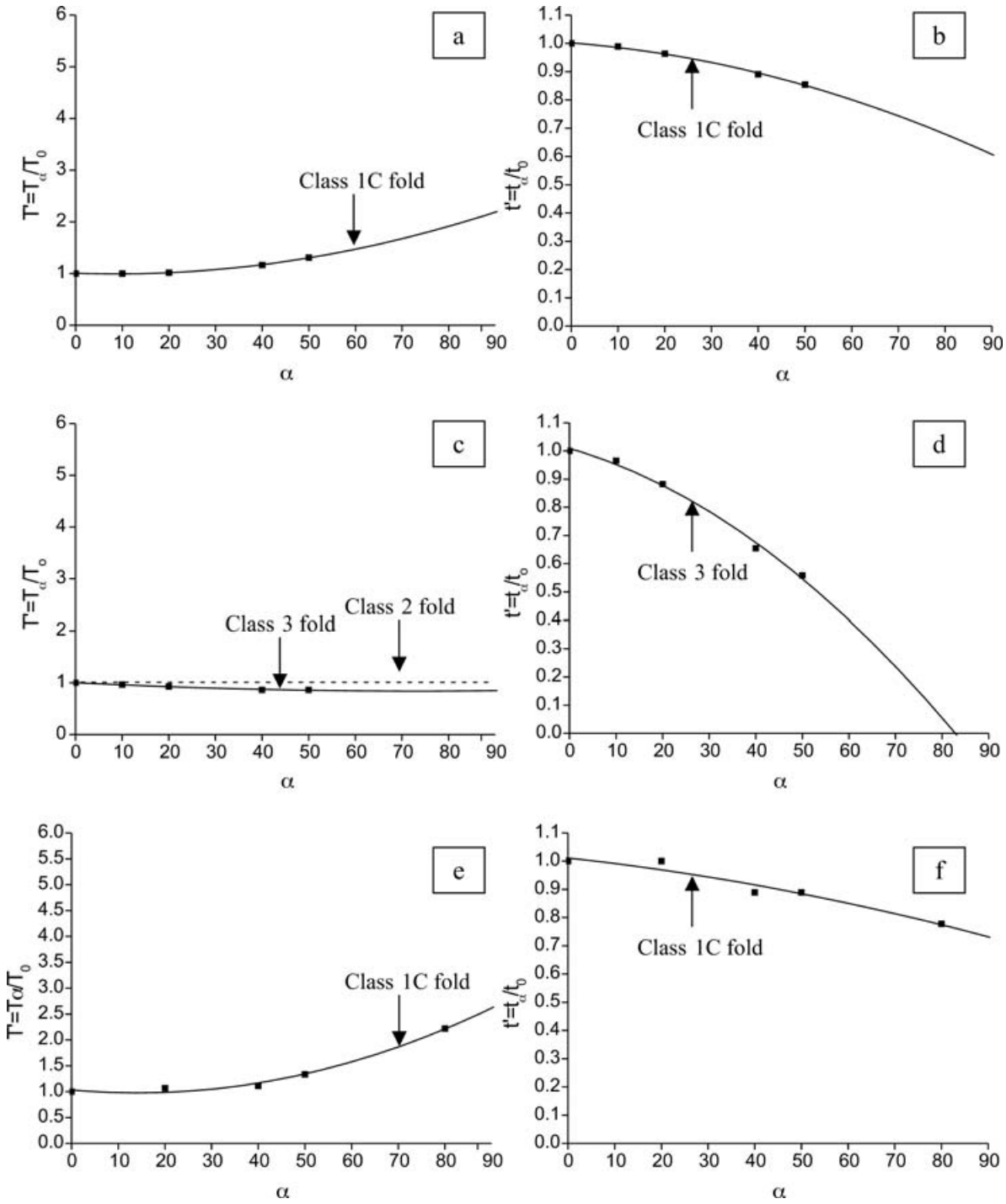

Figure 11. T′ v. α and t′ v. α plots to determine the class of folds developed in the competent and incompetent units of the BIF under investigation. (a, b) are T′ v. α and t′ v. α plots, respectively, for the competent layer (shown by white arrow pointing towards C) in Figure 5a. (c, d) are T′ v. α and t′ v. α plots, respectively, for the incompetent layer (shown by white arrow pointing towards IC) in Figure 5a. (e, f) are the T′ v. α and t′ v. α plots, respectively, for the competent layer (shown by white arrow in top left corner) in Figure 9a. The competent layers have developed class 1C folds as noted from (a), (b), (e) and (f). The incompetent layer developed class 3 folds, documented in (c) and (d).

superposed on tangential longitudinal strain that led to development of class 1C folds in the competent layers. A comparison of the t′ v. α and T′ v. α plots shown in Figure 11 with those given by Ramsay (1967, p. 413, fig. 7–79 and p. 414, fig. 7–80) reveals that the competent layer in Figure 5a has $\sqrt{\lambda_2/\lambda_1} = 0.7$. However, in the competent layer of the fold in Figure 9a, there is a variation in the $\sqrt{\lambda_2/\lambda_1}$ value from the hinge to the limb of the fold; $\sqrt{\lambda_2/\lambda_1} = 0.35$ at the limbs (where $\alpha = 80$) and this value increases to 0.75 at $\alpha = 50$ and is 1.0 close to the hinge of the fold. The $\sqrt{\lambda_1/\lambda_2}$ value is thus calculated to be 2.85 on the limbs

https://doi.org/10.1017/S0016756806002998 Published online by Cambridge University Press

and 1 at the hinge. This implies that the flattening strain was greater at the limb than the hinge in this particular layer, and this superposition modified the class 1B fold to class 1C.

The geometry of microstructures such as quartz strain fringes around folded iron ore layers provides further information regarding the fold mechanism. Figures 9a and 10 reveal that the strain fringe zone is thinner at the limb as compared to the hinge of the fold. Also, the fringes are straight and oblique to the layer at the limb and become increasingly curved towards the hinge of the fold. It is envisaged that during D_2 folding, because of the competence contrast between the different layers of the BIF, flexural-slip was also prevalent at the contact between the competent and incompetent units. While the competent layer folded by tangential longitudinal strain, the incompetent layer folded by flexural flow. In between the competent and incompetent units there was flexural slip. Since strain was accommodated at different rates in individual layers, this may have played an important role in the initial generation of space, which was filled up by quartz fibres. With progressive deformation/folding and associated flexural slip, there was top-towards-hinge sense of movement of the quartz fibres, which would be expected on account of slipping in between layers of differing competence (Figs 9, 10). With progressive growth of the quartz fibres, folding also continued and homogeneous flattening strain was superposed on the earlier strain. It is inferred that the non-orthogonal relationship between this flattening direction and the refracted quartz veins led to the development of drag effect in some parts of the quartz veins (Fig. 5b).

Thus it is concluded that a combination of folding mechanisms, namely buckling by tangential longitudinal strain, flexural-flow, flexural-slip and homogeneous flattening, controlled the development of D_2 folds in the BIF under investigation. Buckling by tangential longitudinal strain in the competent layer and flexural flow in the incompetent layer dominated initially. This led to the formation of refracted fractures close to the outer arc of the folds that form the refracted quartz veins. Flexural-slip was also prevalent during progressive folding at the interface between layers. The combination of these mechanisms led to the development of class 1B folds in the competent layer and class 3 folds in the incompetent layer. With further progressive D_2 deformation, homogeneous flattening became dominant and modified the folds in competent layers to class 1C. However, the class 3 folds remained within class 3 although they do show a tendency to approach class 2 folds, which is in accordance with the suggestion of Ramsay (1962, 1967). That homogeneous flattening played an active role during folding is also supported by (a) ore minerals preferentially oriented in the axial planar direction of D_2 folds (AP_2), which was documented in Figure 4b–c and (b) evidence of pressure solution along thinned limbs of the strain fringe zone in Figure 9a. The latter is particularly interesting because the limb of the folded strain-fringe zone is thinner than the hinge part, and it is noted that there are some fractures in the limb that are occupied by coarse quartz crystals. It is envisaged that pressure solution may have accompanied homogeneous flattening during the later stages of folding. During this process, quartz from the strain-fringe at the limbs migrated to lower-stress regions such as fractures, thus giving the present geometry.

4.d. Growth of strain fringes around core objects

It was shown in Section 3.c.1 that the strain fringes around core objects have grown in a more or less axial planar direction (AP_2, Fig. 8). This relationship provides very useful information about the process that led to the development of strain fringes around the core objects. It is generally believed that fibres grow parallel to the maximum instantaneous stretching axis. This is based on two basic hypotheses: (1) fibre growth takes place parallel to the least stress because crystals have to overcome the smallest stress in this direction (Durney & Ramsay, 1973) and (2) fibres follow asperities on the wall-rock or core object (Urai, Williams & van Roermund, 1991). Koehn *et al.* (2000) carried out numerical simulations of fibre growth in antitaxial strain fringes and found that face-controlled strain fringes grow around smooth core objects, and strain fringes with both displacement-controlled and face-controlled fibres grow around core objects with rough surfaces. Figures 7a–c and 8a–b from the BIF of the present study area show presence of asperities (rough surfaces) to which the strain fringes are attached, thus supporting the inferences made by Koehn *et al.* (2000) from numerical modelling. However, it is also noted that growth of the fringes in samples of the BIF presently investigated is on average parallel to the axial plane direction (Fig. 8), which is a direction perpendicular to maximum principal compressive stress and therefore is the direction of least stress. This also supports the hypothesis of Durney & Ramsay (1973) that fibre growth occurs parallel to the least stress. Also, it is important to note that no fringe growth is observed perpendicular to the axial planar direction of the folds. Therefore, from the present study it would not be wrong to comment that in the BIF under investigation, control of stress on growth of strain fringes is equally as important as the presence of asperities on ore minerals.

4.e. Microscale deformation processes

The identification of successive development of microstructures during different stages of deformation events in the BIF under investigation has helped decipher

https://doi.org/10.1017/S0016756806002998 Published online by Cambridge University Press

the variations that took place in the conditions of deformation and hence the deformation processes.

The presence of bedding-parallel fabric and the absence of undulatory extinction in quartz comprising the quartz layers defining this fabric (Fig. 6a–c) implies that this part of pre-D_2 deformation must have occurred at relatively lower temperatures. These quartz crystals also show presence of interpenetrating grain contacts (shown by white arrow in Fig. 6c). Therefore, it is inferred that diffusive mass transfer by solution was the favoured mechanism during the genesis of bedding-parallel fabric (Passchier & Trouw, 1996, p. 26; Blenkinsop, 2000, p. 25).

The syn-D_2 quartz veins that cut through the bedding-parallel fabric (Fig. 6a–c) are generally devoid of any shape-preferred orientation. The quartz crystals in the veins are coarse and have sharp interpenetrating boundaries (black arrow in Fig. 6c). Therefore, the deposition/precipitation of quartz into these veins is also inferred to have taken place by diffusive mass transfer by solution. However, since some of the quartz crystals in these veins also show undulatory extinction and bulging irregular grain boundaries (Fig. 6d), it is inferred that some quartz crystals were subjected to intracrystalline deformation.

D_2 deformation resulted in the growth of strain fringes around rigid iron oxide core objects as well as adjacent to folded iron ore layers. Since the strain fringes are oriented parallel to D_2 fold axial planes (AP_2), it is inferred that they are synkinematic with D_2. Development of strain fringes is considered to indicate diffusive mass transfer by solution (Passchier & Trouw, 1996, p. 141; Blenkinsop, 2000, p. 33). During the formation of these strain fringes by diffusive mass transfer, dilation of the strain fringe, transport of material to the strain fringe and precipitation of material and growth of quartz crystals in the strain fringe must have been the three important processes; the relative rates at which transport, dilation and precipitation processes operate may have had a strong influence on the microstructure of strain fringes (Fisher & Brantley, 1992; Bons & Jessel, 1997; Hilgers *et al.* 2001). However, quartz crystals that comprise strain fringes also show undulatory extinction and bulging irregular grain boundaries (Fig. 7b, c), and a few quartz crystals in the same sample have also developed subgrains (Fig. 7d); all these imply dynamic recrystallization by bulging. Moreover, it was shown above that quartz fibres around folded iron ore layers also developed during D_2 (Fig. 9) and this also necessitates diffusive mass transfer as an important mechanism for their initiation. However, the presence of undulatory extinction in some of the fibres implies that they also underwent intracrystalline deformation during D_2. Simultaneous operation of different processes during a particular deformation is not unlikely in nature and has been demonstrated in some earlier studies (e.g. Hippertt, Lana & Takeshita, 2001; Mamtani, Karanth & Greiling, 1999; Lagoeiro, Hippertt & Lana, 2003). The present study also indicates that different deformation processes were simultaneously operational. It is inferred that diffusive mass transfer by solution, intracrystalline deformation and associated bulging dynamic recrystallization were the important processes that operated during the deformation of the BIF of the Bonai Synclinorium. It may also be noted that the deformation was fluid-assisted because (a) fluid inclusion planes are noted in some of the quartz fringes that are oriented parallel to the fold axial trace (AP_2) and (b) fluid inclusions are also present along grain boundaries of recrystallized quartz crystals (Fig. 12a–d).

4.f. Estimation of temperature and strain rate

Das *et al.* (1996) stated that the BIFs of the Bonai Synclinorium were not subjected to temperatures above 200 °C. However, the presence of bulging quartz grain boundaries implies a temperature range of 280–400 °C (Stipp *et al.* 2002*a*,*b*). At temperatures as high as 400 °C, the jasper that comprises the competent layers in the BIF would have been extensively recrystallized, which is not observed. Therefore, it can be safely concluded that the temperatures during deformation did not reach 400 °C but were definitely greater than 280 °C, which is contrary to the conclusions of Das *et al.* (1996). The authors infer that temperatures between 300 and 350 °C must have been reached to allow the development of dynamic recrystallization microstructures such as bulging grain boundaries as well as some subgrains (Fig. 7d).

It is known that microstructures in rocks depend on the dominance of deformation processes, strain rate ($\dot{\varepsilon}$) and temperature (T) (e.g. Hirth & Tullis, 1992; Piazolo *et al.* 2002; Stipp *et al.* 2002*a*,*b*). Hirth & Tullis (1992) experimentally determined three dislocation creep regimes and associated microstructures in quartz aggregates, namely low T/high $\dot{\varepsilon}$ (regime 1), medium T/medium $\dot{\varepsilon}$ (regime 2) and high T/low $\dot{\varepsilon}$ (regime 3). Stipp *et al.* (2002*a*) proposed three dynamic recrystallization zones using microstructures observed in quartz in the Tonale fault zone (Italian Alps), namely bulging recrystallization (BLG; 280–400 °C), subgrain rotation (SGR; 400–500 °C) and grain boundary migration (GBM; 500–700 °C). Moreover, Stipp *et al.* (2002*b*) correlated dynamic recrystallization microstructures in quartz developed under natural conditions with the experimental results of Hirth & Tullis (1992) for water-added samples based on which a T/$\dot{\varepsilon}$ diagram was proposed. Piazolo *et al.* (2002) used the numerical model 'ELLE' to evaluate the influence of different processes on microstructure development and dynamic recrystallization of quartz. They proposed three groups of microstructures based on the dominant process responsible for their development,

https://doi.org/10.1017/S0016756806002998 Published online by Cambridge University Press

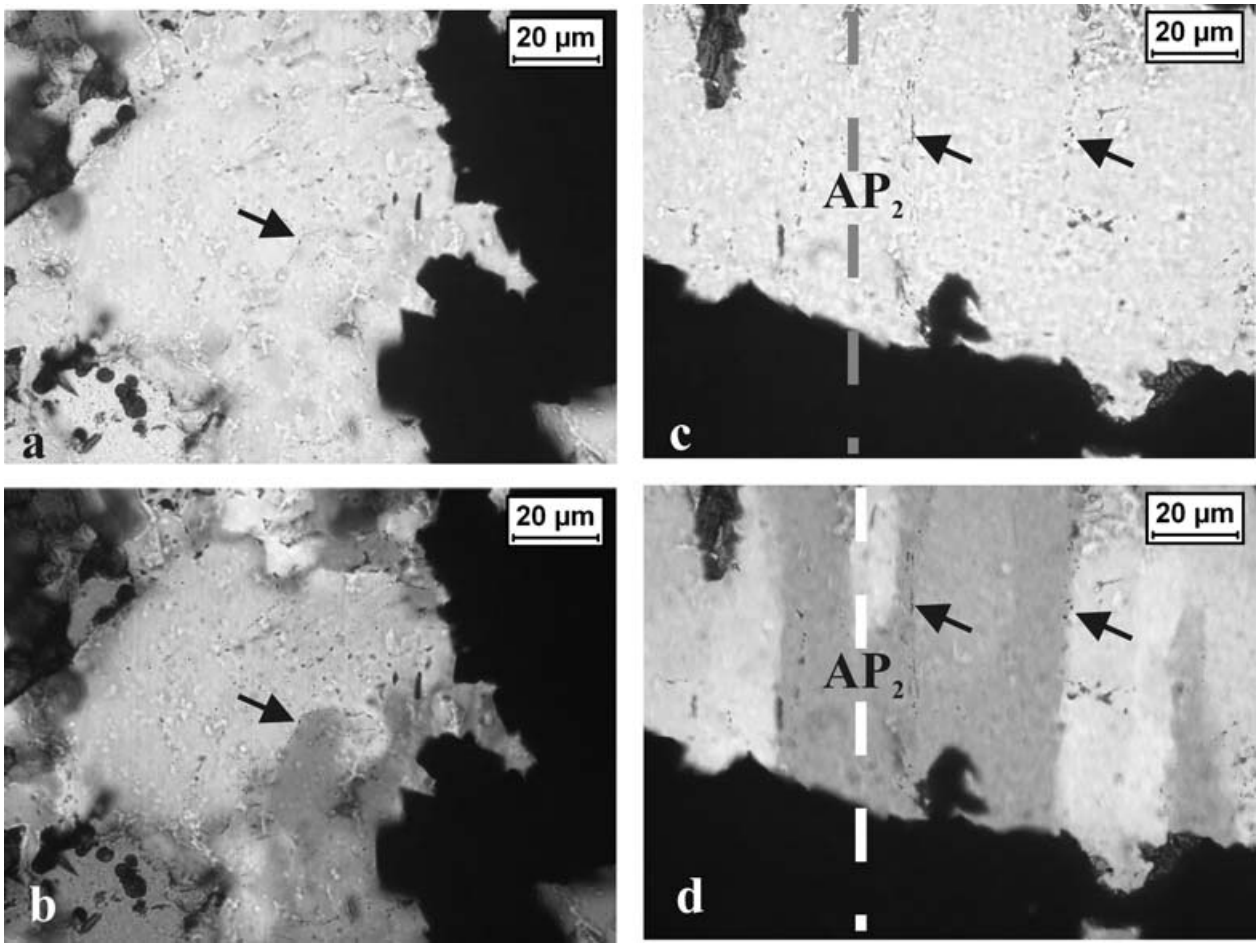

Figure 12. Photomicrographs documenting the presence of fluid inclusions in quartz crystals in the BIFs of Gua mine (India). These imply that the deformation and recrystallization were fluid-assisted and were not under dry conditions. (a, b) Photomicrographs taken in plane polarized light (PPL) and partially crossed nicols, respectively, and arrows in these point to fluid inclusions at grain boundary of quartz. (c) and (d) are also photomicrographs taken under plane polarized light and partially crossed nicols, respectively. Arrows point to fluid inclusion trails at grain boundaries of quartz strain fringes. The orientation of fluid inclusion trails is parallel to the AP_2 direction.

grain boundary mobility (M_{gb}) and energy threshold value for nucleation (τ_{nucl}). Group A microstructures require high τ_{nucl}, low M_{gb} and rotation recrystallization and recrystallization by nucleation with no significant grain boundary migration. Group B microstructures are characterized by high τ_{nucl}, medium M_{gb}, dominating recrystallization by nucleation and limited grain boundary migration. Group C microstructures are dominated by grain boundary migration and have very high M_{gb}. The reader is referred to Table 4 of Piazolo *et al.* (2002) for a detailed comparison of conditions, features and interpretation of the above three groups with those proposed by Hirth & Tullis (1992) and Stipp *et al.* (2002*a*). Accordingly, the quartz microstructures observed in the BIF of the study area fall under regime 1 of Hirth & Tullis (1992), BLG zone of Stipp *et al.* (2002*b*) and Group A of Piazolo *et al.* (2002).

In addition to the above, deformation microstructure maps have been proposed for quartz which permit an estimation of strain rate if the dynamic recrystallization mechanism and temperature conditions are known (Piazolo *et al.* 2002; Stipp *et al.* 2002*b*). According to Piazolo *et al.* (2002), the grain mobility as well as temperature of nucleation can also be estimated from such maps. It has been shown above that the BIF under investigation underwent bulging recrystallization at temperatures of around 300–350 °C. With this database a $\dot{\varepsilon}$ of the order of 10^{-14} to 10^{-12} s^{-1} is estimated using the recrystallization mechanism map of Stipp *et al.* (2002*b*) (Fig. 13a). The quartz microstructures of the present study fall in the category of Group A microstructures of Piazolo *et al.* (2002), which requires a low grain boundary mobility (M_{gb}) and high-energy threshold value for nucleation (τ_{nucl}). Using the deformation microstructure map of Piazolo *et al.* (2002) for a temperature of 300–350 °C, a $\dot{\varepsilon}$ of the order of $\sim 10^{-12}$ s^{-1} is estimated (Fig. 13b). $\dot{\varepsilon}$ for natural geological deformation is very similar to the above estimated range (Twiss & Moores, p. 382; Stipp *et al.* 2002*b*). Therefore the T/$\dot{\varepsilon}$ regime estimates of 300–350 °C/10^{-14}–10^{-12} s^{-1} from the observed microstructures in the BIF of the Bonai Synclinorium are quite realistic.

https://doi.org/10.1017/S0016756806002998 Published online by Cambridge University Press

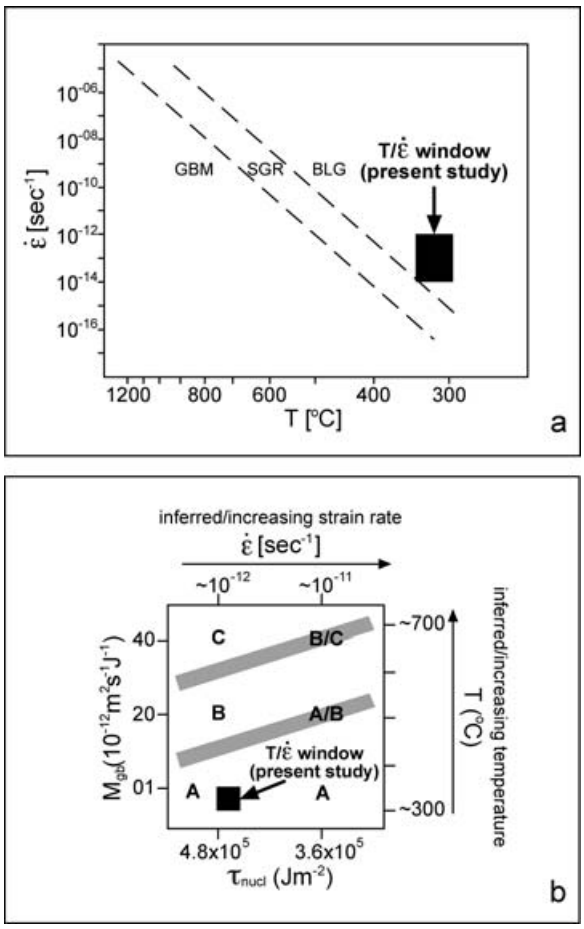

Figure 13. Estimation of strain rate ($\dot{\varepsilon}$) from the quartz microstructures observed in the BIF of Gua mine. (a) T/$\dot{\varepsilon}$ window for the present study on the recrystallization mechanism map proposed by Stipp *et al.* (2002*b*). BLG, SGR and GBM, respectively, represent dynamic recrystallization by bulging, subgrain rotation and grain boundary migration. (b) T/$\dot{\varepsilon}$ window for the present study on the deformation microstructure map proposed by Piazolo *et al.* (2002). M_{gb} is grain boundary mobility and τ_{nucl} is the energy threshold value for nucleation. The T/$\dot{\varepsilon}$ values inferred from both the maps are comparable and are estimated to be 300–350 °C/10^{-14}–10^{-12} s^{-1} (see Section 4.f for detailed discussion).

5. Conclusions

Microstructural studies on BIFs are scarce. Moreover, investigations involving an integrated evaluation of microstructure development, operative microstructural processes, their time relationship with folding and mechanism of folding have rarely been attempted on folded rocks, especially BIFs. The present study has demonstrated that BIFs can preserve a plethora of information about deformation processes, temperature, strain rate and mechanisms of folding. The following conclusions are arrived at with regards to the BIF of the Gua mine (Bonai Synclinorium, eastern India).

(1) The BIF of Gua mine has a pre-D_2 bedding-parallel fabric defined by flattened quartz crystals that is transected by quartz veins occupying refracted fractures forming convergent and divergent fans. The refracted quartz veins developed synchronously with D_2 folding.

(2) Folding of the BIF occurred by a combination of mechanisms. Tangential longitudinal strain and flexural flow dominated in the competent and incompetent layers, respectively. Flexural slip occurred at the interface between layers of differing competence. These led to development of class 1B folds in the competent layer and class 3 folds in the incompetent layer and the development of convergent and divergent cleavage fans. With progressive folding, homogeneous flattening strain was superimposed on the earlier strain as a result of which the competent layers were modified to class 1C folds. This superposition was greater on the limbs than the hinges of respective folds.

(3) Quartz strain fringes around rigid iron oxide core objects are antitaxial and are oriented subparallel to the axial planar direction of D_2 folds. This implies growth of fringes in the direction of least stress, that is, perpendicular to the maximum compressive stress, which is in accordance with the suggestion of Durney & Ramsay (1973). Besides this, all the core objects observed in the BIF samples have rough surfaces (asperities) and have a combination of face-controlled and displacement-controlled growth fibres, which also supports the suggestion of Koehn *et al.* (2000).

(4) Diffusive mass transfer by solution was an important process, which led to the development of strain fringes as well as the formation of dentate grain boundaries in quartz crystals that comprise the bedding-parallel shape fabric and refracted quartz veins.

(5) Dynamic recrystallization by bulging also operated along with diffusive mass transfer by solution. This resulted in the development of irregular bulging grain boundaries and subgrains in some of the quartz crystals.

(6) The temperatures during deformation of the BIF are inferred to have been ~ 300–350 °C, which is greater than the previously proposed temperature of < 200 °C (Das *et al.* 1996).

(7) A strain rate of the order of 10^{-14}–10^{-12} s^{-1} is estimated using the deformation microstructure maps of Piazolo *et al.* (2002) and Stipp *et al.* (2002*b*); this strain rate is realistic for natural geological deformation processes.

Acknowledgements. Comments and suggestions by D. W. Durney on an earlier version of the manuscript are gratefully acknowledged. Reviews by two anonymous journal referees and suggestions during revision by H. B. Srivastava, D. C. Srivastava and Saibal Gupta were found useful. Editorial suggestions by Mark Allen, J. Imber and Mrs Jane

Holland are acknowledged. However, the authors take all responsibility for the interpretations made in this paper.

References

BLENKINSOP, T. J. 2000. *Deformation microstructures and mechanisms in minerals and rocks*. Dordrecht: Kluwer Academic Publishers, 150 pp.

BONS, P. D. & JESSEL, M. W. 1997. Experimental simulation of the formation of fibrous veins by localized dissolution–precipitation creep. *Mineralogical Magazine* **61**, 53–63.

CASTRO, L. 1994. Genesis of BIF. *Economic Geology* **89**, 1384–97.

CHAUVET, A., FAURE, M., DOSSIN, I. & CHARVET, J. 1994. A three-stage structural evolution of the Quadrilátero Ferrífero: consequences for the Neoproterozoic age and the formation of gold concentrations of the Ouro Preto area, Minas Gerias, Brazil. *Precambrian Research* **68**, 139–67.

CHEMALE, F. Jr, ROSIÈRE, C. A. & ENDO, I. 1994. The tectonic evolution of the Quadrilátero Ferrífero, Minas Gerais. *Precambrian Research* **65**, 25–54.

DAS, A. K., PIPER, J. D. A., MALLIK, S. B. & SHERWOOD, G. J. 1996. Palaeomagnetic study of Archaean Banded Hematite Jasper Rocks from the Singhbhum-Orissa Craton, India. *Precambrian Research* **80**, 193–204.

DURNEY, D. W. & RAMSAY, J. G. 1973. Incremental strains measured by syntectonic crystal growths. In *Gravity and Tectonics* (eds K. A. DeJong and R. Scholten), pp. 67–95. New York: Wiley.

ETCHECOPAR, A. & MALAVIELLE, J. 1987. Computer models of pressure shadows: a method for strain measurement and shear sense determination. *Journal of Structural Geology* **9**, 667–77.

FISHER, D. M. & BRANTLEY, S. L. 1992. Models of quartz overgrowth and vein formation: deformation and episodic fluid flow in an ancient subduction zone. *Journal of Geophysical Research* **97**, 20043–61.

GHOSH, S. K. 1993. *Structural Geology. Fundamentals and Modern Developments*. Oxford: Pergamon Press, 598 pp.

HILGERS, C., KOEHN, D., BONS, P. D. & URAI, J. L. 2001. Development of crystal morphology during unitaxial growth in a progressively widening vein: II. Numerical simulations of the evolution of antitaxial fibrous veins. *Journal of Structural Geology* **23**, 873–85.

HIPPERTT, J., LANA, C & TAKESHITA, T. 2001. Deformation partitioning during folding of banded iron formation. *Journal of Structural Geology* **23**, 819–34.

HIRTH, G. & TULLIS, J. 1992. Dislocation creep regimes in quartz aggregates. *Journal of Structural Geology* **14**, 145–60.

JONES, H. C. 1934. The iron ores of Bihar and Orissa. *Geological Survey of India Memoir* **63**, 167–302.

KOEHN, D., AERDEN, D. G. A. M., BONS, P. D. & PASSCHIER, C. W. 2001. Computer experiments to investigate complex fibre patterns in natural antitaxial strain fringes. *Journal of Metamorphic Geology* **19**, 217–31.

KOEHN, D., BONS, P. D. & PASSCHIER, C. W. 2003. Development of antitaxial strain fringes during non-coaxial deformation: an experimental study. *Journal of Structural Geology* **25**, 263–75.

KOEHN, D., HILGERS, C., BONS, P. D. & PASSCHIER, C. W. 2000. Numerical simulation of fibre growth in antitaxial strain fringes. *Journal of Structural Geology* **22**, 1311–24.

LAGOEIRO, L., HIPPERTT, J. & LANA, C. 2003. Deformation partitioning during folding and transposition of quartz layers. *Tectonophysics* **361**, 171–86.

MAJUMDAR, T. & CHAKRABORTY, K. L. 1979. Petrography and petrology of the Precambrian Banded Iron Formation of Orissa, India and reformation of the bands. *Sedimentary Geology* **22**, 243–65.

MAMTANI, M. A., KARANTH, R. V. & GREILING, R. O. 1999. Are crenulation cleavage zones mylonites on the microscale? *Journal of Structural Geology* **21**, 711–18.

MUKHERJI, A., CHAUDHURI, A. K. & MAMTANI, M. A. 2004. Regional scale strain variations in the Banded Iron Formations of Eastern India: results from Anisotropy of Magnetic Susceptibility studies. *Journal of Structural Geology* **26**, 2175–89.

PASSCHIER, C. W. & TROUW, R. A. J. 1996. *Microtectonics*. Heidelberg: Springer-Verlag, 289 pp.

PIAZOLO, S., BONS, P. D., JESSELL, M. W., EVANS, L. & PASSCHIER, C. W. 2002. Dominance of microstructural processes and their effect on microstructural development: insights from numerical modeling of dynamic recrystallisation. In *Deformation Mechanisms, Rheology and Tectonics: Current Status and Future Perspectives* (eds S. de Meer, M. R. Drury, J. H. P. de Bresser and G. M. Pennock), pp. 149–70. Geological Society of London, Special Publication no. 200.

RAMSAY, J. G. 1962. The geometry and mechanics of formation of "similar" type folds. *Journal of Geology* **70**, 309–27.

RAMSAY, J. G. 1967. *Folding and Fracturing of Rocks*. New York: McGraw-Hill Book Company, 560 pp.

RAMSAY, J. G. & HUBER, M. I. 1983. *The Techniques of Modern Structural Geology, Vol. 1: Strain Analysis*. London: Academic Press, 307 pp.

RAMSAY, J. G. & HUBER, M. I. 1987. *The Techniques of Modern Structural Geology, Vol. 2: Folds and Fractures*. London: Academic Press, pp. 309–700.

RAMSAY, J. G. & LISLE, R. J. 2000. *The Techniques of Modern Structural Geology, Vol. 3: Applications of continuum mechanics in structural geology*. London: Academic Press, pp. 702–1061.

ROSIÈRE, C. A., SIEMES, H., QUADE, H., BROKMEIER, H.-G. & JANSEN, E. M. 2001. Microstructures, textures and deformation mechanisms in hematite. *Journal of Structural Geology* **23**, 1429–40.

SAHA, A. K. 1994. Crustal Evolution of Singhbhum-North Orissa Eastern India. *Geological Society of India Memoir* **27**, 341 pp.

SAHA, A. K., RAY, S. L. & SARKAR, S. N. 1988. Early history of the earth: evidence from the eastern Indian shield. In *Precambrian of the eastern Indian shield* (ed. D. Mukhopadhyay), pp. 13–37. Geological Society of India, Memoir no. 8.

SIEMES, H., KLINGENBERG, B., RYBACKI, E., NAUMANN, M., SCHÄFER, W., JANSEN, E. & ROSIÈRE, C. A. 2003. Texture, microstructure, and strength of hematite ores experimentally deformed in the temperature range 600–1100 °C and at strain rates between 10–4 and 10–6. *Journal of Structural Geology* **25**, 1371–91.

STIPP, M., STÜNITZ, H., HEILBRONNER, R. & SCHMID, S. M. 2002*a*. The eastern Tonalite fault zone: a 'natural laboratory' for crystal plastic deformation of quartz

over a temperature range from 250–700 °C. *Journal of Structural Geology* **24**, 1861–84.

STIPP, M., STÜNITZ, H., HEILBRONNER, R. & SCHMID, S. M. 2002*b*. Dynamic recrystallisation of quartz: correlation between natural and experimental conditions. In *Deformation Mechanisms, Rheology and Tectonics: Current Status and Future Perspectives* (eds S. de Meer, M. R. Drury, J. H. P. de Bresser and G. M. Pennock), pp. 171–90. Geological Society of London, Special Publication no. 200.

STOLZ, J. F., LOVELY, D. R. & HAGGERTY, S. E. 1990. Biogenic magnetite and the magnetisation of sediments. *Journal of Geophysical Research* **95**, 4355–62.

TREAGUS, S. H. 1983. A theory of strain variation through contrasting layers, and its bearing on cleavage refraction. *Journal of Structural Geology* **5**, 351–68.

TWISS, R. J. & MOORES, M. E. 1992. *Structural Geology*. New York: W. H. Freeman and Company, 532 pp.

URAI, J. L., WILLIAMS, P. F. & VAN ROERMUND, H. L. M. 1991. Kinematics of crystal growth in syntectonic fibrous veins. *Journal of Structural Geology* **13**, 823–36.